Synthesis of atomically layered and chemically ordered Rare-Earth (RE) *i*-MAX phases; $(Mo_{2/3}RE_{1/3})_2GaC$ with RE = Gd, Tb, Dy, Ho, Er, Tm, Yb, and Lu

Andrejs Petruhins, Jun Lu, Lars Hultman, Johanna Rosen

Thin Film Physics Division, Department of Physics, Chemistry and Biology (IFM), Linköping University, SE-581 83 Linköping, Sweden

Abstract

We report synthesis of eight new members of the *i*-MAX family, of the formula $(Mo_{2/3}RE_{1/3})_2GaC$, where RE = Gd, Tb, Dy, Ho, Er, Tm, Lu, and Yb, the latter not previously incorporated in a MAX phase. The structure and composition of powder samples were investigated by X-ray diffraction, scanning transmission electron microscopy, and energy dispersive X-ray analysis combined with scanning electron microscopy. All phases showed evidence of an orthorhombic (*Cmcm*) structure, and the phases based on Er and Yb also crystallized in a monoclinic (*C*2/*c*) arrangement. The chemical order of the magnetic elements suggests interesting magnetic characteristics, with a high tuning potential through the range of attainable lanthanide elements.

Impact statement

We present eight new in-plane ordered *i*-MAX phases based on rare earth elements, including Yb (new MAX phase element), with high magnetic characteristics tuning potential.

Keywords: *i*-MAX phase, atomic laminate, chemical order, materials synthesis, rare earth elements, magnetism

Introduction

Chemical ordering of magnetic elements in a material sits at the crossroad of fascinating condensed matter physics, giving rise to phenomena such as the anomalous Hall effect and multiferroicity [1, 2]. Furthermore, rare earth (RE) elements are known to exhibit various magnetic and electronic ground states, owing to hybridization of 4*f* and conduction electrons [3, 4, 5]. Heavy fermion systems being complex are excellent systems to study interactions between magnetic and valence instabilities[6]. These are also useful systems to study quantum phase transitions [7] and complex collective quantum states [8]. When the ions are surrounded by the free electrons, the interaction among the *f* shells is dominated by indirect exchange coupling between the localized spins, the Ruderman–Kittel–Kasuya–Yosida (RKKY) interaction [9, 10, 11], giving rise to long-range magnetic order. Heavy fermion states in some lanthanides can lead to interesting magnetic states, including metamagnetic-like transitions [5, 8, 12].

Recently, a family of quaternary atomic laminates were discovered, coined *i*-MAX phases [13, 14]. They stem from so called MAX phases, which are a family of atomic nanolaminates with general formula $M_{n+1}AX_n$, where *M* is a transition metal, *A* is an A-group element and *X* is C or N, $n = 1 – 3$ [15]. First discovered in the 1960s [16] and further extensively studied in the 1990s [17] and onwards, MAX phases have been attractive study topic due to their combination of metallic and ceramic properties [18] with remarkable mechanical properties [19]. These properties make the materials suitable for various applications, such as nuclear reactor applications [20], ohmic contacts [21], and precursors for synthesis of their 2D counterparts – Mxenes [22, 23].

Different to MAX phases, the *i*-MAX phases display in-plane chemical ordering of two different M-elements, as described by the general formula $(M^1_{2/3}M^2_{1/3})_2AC$, wherein the M^1

atoms form a honeycomb lattice and the M^2 atoms a triangular lattice. Furthermore, the A-layer is arranged in a Kagomé-like structure. For a more detailed description, see Refs. [14, 24]. To date, *i*-MAX phases with A= Al and Ga have been reported, where X is C. Notably, the discovery of *i*-MAX phases has significantly expanded the number of M elements used in MAX-phases, for example through M = Y and W [25, 26]. Furthermore, the *i*-MAX phases have been shown to realize a new type of MXenes with either in-plane chemical order or vacancy-ordering [13, 25, 27], with shown high potential for energy storage.

Most recently, the discovery of 11 new *i*-MAX phases was reported, including rare-earth (RE) elements and being of the general formula $(Mo_{2/3}RE_{1/3})_2AlC$ [28], where RE = Ce, Pr, Nd, Sm, Gd, Tb, Dy, Ho, Er, Tm, and Lu. It was shown that these phases can display three different but similar symmetries; monoclinic (*C*2/*c*), monoclinic (*C*2/*m*), and orthorombic (*Cmcm*). Furthermore, analysis of RE-*i*-MAX phases with Nd, Gd, Tb, and Er indicated complex magnetic ordering, being sensitive to temperature and applied magnetic field, which is characteristics of frustrated systems. This recent study has served as a motivation for the present work, and herein we report the synthesis and structural characterization of eight new *i*-MAX compounds of the general formula $(Mo_{2/3}RE_{1/3})_2GaC$, for which RE = Gd, Tb, Dy, Ho, Er, Tm, Yb, and Lu. The realized phases add a new element to the MAX phase family (Yb), and serve as inspiration for continued systematic studies on effect of RE element on the magnetic properties. The compounds also allow detailed studies on the effect of A-element on the overall magnetic characteristics.

Methods

Materials synthesis

Polycrystalline samples of $(Mo_{2/3}RE_{1/3})_2GaC$, where RE = Gd, Tb, Dy, Ho, Er, Tm, Yb, and Lu, were synthesized by solid-state reaction from elemental constituents. Elemental powders of Mo (99.99%) and graphite (99.999%), from Sigma Aldrich, were used together with the RE elements (99.5%), the latter from Stanford Advanced Materials. For Ga, metal pellets (99.99999%), from Mining and Chemical Products Limited, of about 7 mm diameter and of mass ~1 g were used, after being mechanically cleaved into smaller pieces of about 1 mm in diameter. The Mo:RE:Ga:C were mixed in a stoichiometric ratio of 4:2:3:3. First, Mo, RE and C powders were mechanically mixed in an agate mortar. The powder mixture was then placed in an alumina crucible, Ga pellets were added, and the pellet/powder mixture was stirred. The alumina crucible with its content was thereafter heated under five standard cubic centimeter per minute (sccm) Ar flow to 1400 °C at a rate of 10 °C/min, and then held at 1400 °C for 5 h. The loosely sintered powders were crushed into a fine powder that was directly used for further analysis.

Structural characterization

X-ray diffraction (XRD) analysis of powder samples were performed using a Panalytical X'pert powder diffractometer using Cu Kα radiation (λ = 1.54 Å), equipped with Bragg-Brentano HD on incident side with 1/4° divergence slit and 1/2° anti-scatter slit. On the diffracted beam side, a 5-mm anti-scatter slit together with a Soller slit (with an opening radius of 0.04) was used. A continuous scan from 5° to 120° was performed on the sample with step size of 0.008° and counting time of 60 s per step. XRD Rietveld refinement using FullProf Suite [29, 30] was used to evaluate the sample's phase purity.

Specimens for scanning transmission electron microscopy (STEM) analysis were prepared by dispersing powder on Cu grid with C film. STEM combined with high angle annular dark field imaging (STEM-HAADF) and selected area electron diffraction (SAED) was performed in the double-corrected Linköping FEI Titan^3, operated at 300 kV. Scanning electron microscopy (SEM) analysis was performed using a LEO 1550 SEM operated at 20 kV accelerating voltage, combined with energy dispersive X-ray spectroscopy (EDS) analysis with an Oxford Instruments X-Max 80 mm^2 SDD detector.

Results and discussion

All of the synthesized RE *i*-MAX phases were found to crystallize in a structure of orthorhombic (*Cmcm*) symmetry, however presence of monoclinic (*C*2/*c*) phase was also found in the Er and Yb samples. For details of these structures, see figure S1 in the supplementary information. The $(Mo_{2/3}Tm_{1/3})_2GaC$ *i*-MAX phase was found to be one of highest purity and was thus chosen as a model system for space group #63 (*Cmcm*), shown in figure 1. There, STEM images of the *i*-MAX phase along the (a) [100] and (b) [010] zone axes are shown along with schematic atomic arrangements of the structure based on an orthorombic structure of space group *Cmcm*. The Tm atoms, having the highest atomic number, are the brightest ones due to the *Z*-contrast in STEM, with Ga and Mo appearing less bright (C is not visible). The view of the *i*-MAX along the [100] zone axis is identical to the classical MAX phase when viewed along the [11-20] zone axis. Along the [010], the chemical ordering characteristic of the *i*-MAX phase is evident, where the Tm atoms extend from the Mo layer towards the Ga layer. The Ga layer is arranged in a Kagomé structure, concluded from the alternating contrast between neighboring Ga atoms in the [010] orientation, as seen in figure 1b. The SEM-EDX analysis of the $(Mo_{2/3}Tm_{1/3})_2GaC$ sample gives the relative

composition of 44, 22 and 34 at% for Mo, Tm and Ga, respectively. The XRD data together with Rietveld refinement is shown in figure 1c, and it supports the orthorhombic symmetry (*Cmcm*) as determined from STEM and SAED. The goodness of fit (χ^2) and RF-factor for the *i*-MAX phase values are 22.1 and 7.7, respectively. The goodness of fit and RF-factors for all other samples can be found in table S1 in supplementary information. The quantitative analysis of the sample shows that the *i*-MAX is the main phase, with a small amount of Mo_2C, Tm_2O_3, and $TmGa_3$ impurities. The RE oxide is present in all samples of the present paper, likely originating from a reaction between the alumina crucible and the constituent powder at the sintering temperature. The summary and estimated phase composition of all *i*-MAX containing samples can be found in Table 1, except for the sample for RE=Gd (due to low sample purity). Attempts were also made to synthesize also $(Mo_{2/3}RE_{1/3})_2GaC$ *i*-MAX phase where RE = La, Ce, Pr, Nd, and Sm, however, no *i*-MAX phase could be identified for these elements.

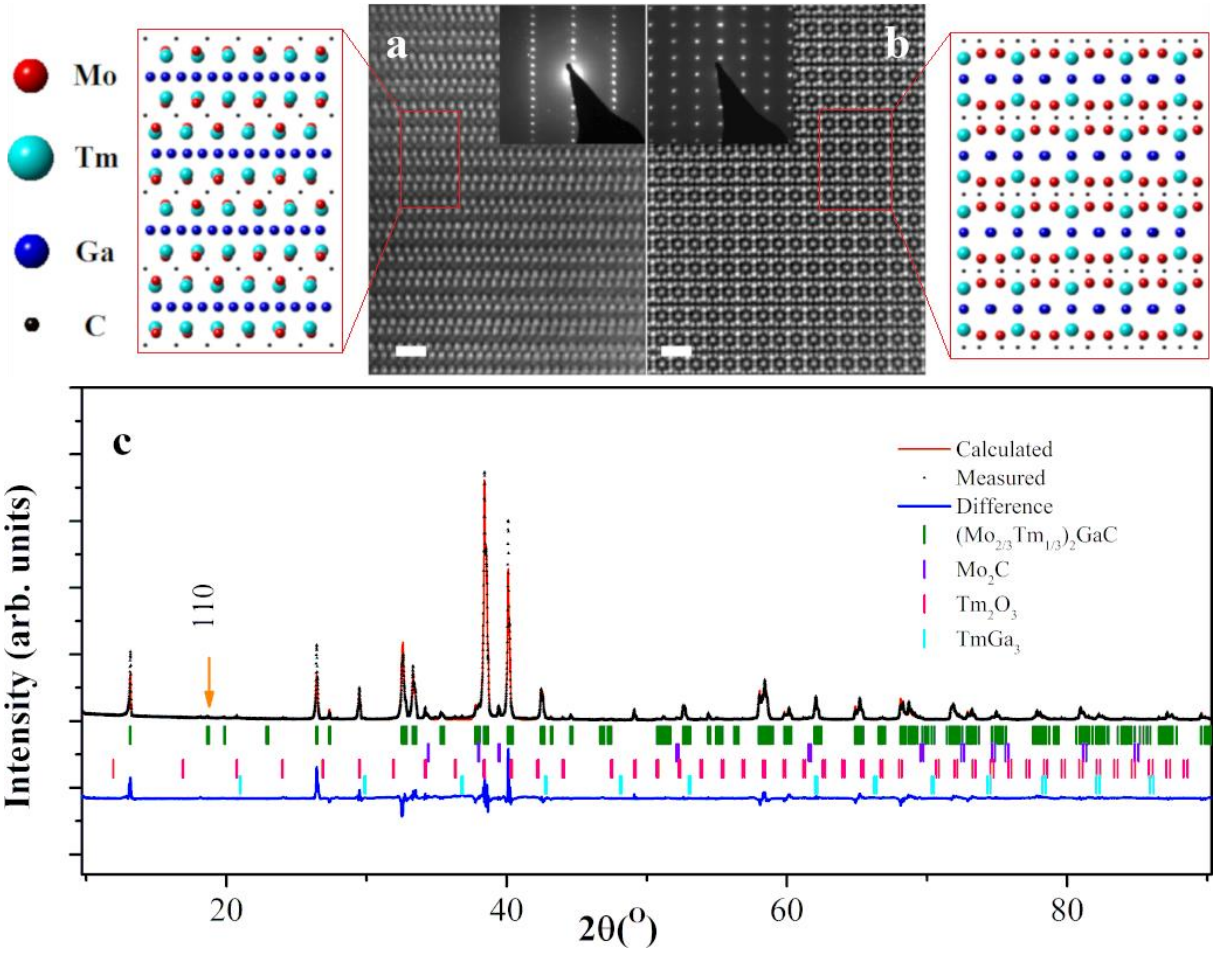

Figure 1. STEM micrographs of $(Mo_{2/3}Tm_{1/3})_2GaC$ *i*-MAX phase along a) [100] and b) [010] zone axis. Insets in panels of a) and b) show SAED from respective orientation. Schematics next to each panel represent the corresponding atomic arrangements assuming a structure with orthorhombic symmetry (*Cmcm*). The scale bars in a) and b) correspond to 1 nm. c) XRD pattern and Rietveld refinement (calculated) of $(Mo_{2/3}Tm_{1/3})_2GaC$, including identified impurity phases.

	Mass fraction of the sample (fraction in wt. %)					Lattice parameters of the *i*-MAX phase (Å)		
RE	*i*-MAX	Mo_2C	C (graphite)	RE_2O_3	$REGa_3$	**a, Å**	**b, Å**	**c, Å**
Gd	-	-	-	-	-	9.613	5.510	13.566
Tb	68.4	13.5	13.0	4.1	1.0	9.580	5.493	13.538
Dy	69.3	8.2	10.1	7.9	4.5	9.560	5.481	13.517
Ho	93.1	0.6	-	2.3	4.0	9.548	5.474	13.505
Er	75.6	6.6	8.1	5.3	4.4	9.529	5.464	13.482
Tm	88.4	4.1	-	7.5	-	9.523	5.459	13.483
Yb	74.5	12.0	7.5	1.6	4.4	9.497	5.454	13.457
Lu	66.4	10.3	11.2	3.4	8.7	9.499	5.446	13.443

Table 1. Phase composition of different samples as quantitatively estimated from Rietveld refinement. The estimated relative uncertainty for the composition is about ±4%. It should be noted that the graphite content might be overestimated in the phase analysis from XRD due to the graphite peak overlapping with the *i*-MAX peak. The structural parameters were determined based on the (*Cmcm)* structure, since the (*C*2/*c*) structure was found as minority phase in only two of the samples. The lattice parameters of the *i*-MAX phases were determined from the Rietveld refinement. Lattice parameters are rounded up to 3 decimal places. Lattice parameter uncertainties from refinement are 0.001 or less for all lattice parameters listed.

Table 1 shows the lattice parameters of the *i*-MAX phases determined from Rietveld refinement, see XRD patterns and, where possible, also the refined data in Figure S2. A clear trend emerges, where all lattice parameters, a, b, and c decrease with increasing atomic number going from Gd to Lu, with $(Mo_{2/3}Gd_{1/3})_2GaC$ having the largest unit cell and $(Mo_{2/3}Lu_{1/3})_2GaC$ the smallest one out of the materials presented herein. The structural parameters were determined based on a (*Cmcm*) structure.

Figure 2 shows STEM micrographs of $(Mo_{2/3}Yb_{1/3})_2GaC$ in the (*C*2/*c*) structure. This atomic arrangement was also found in the sample where RE=Er, though only as a minority phase. Both the (*Cmcm*) and the (*C*2/*c*) structures consist of alternating layers of $(Mo_{2/3}RE_{1/3})_2C$ and Ga building blocks where $(Mo_{2/3}RE_{1/3})_2C$ can have three different orientations; A, B (rotated +60° relative A), and C (rotated +180° relative to A). Different stacking sequences of $(Mo_{2/3}RE_{1/3})_2C$ result in a (*C*2/*c*) structure with ABAB stacking, and a (*Cmcm*) structure with ACAC stacking. Nonetheless, also figure 2 shows the characteristic *i*-MAX features of both the M-element ordering and the indicated rearrangement of the A-layer.

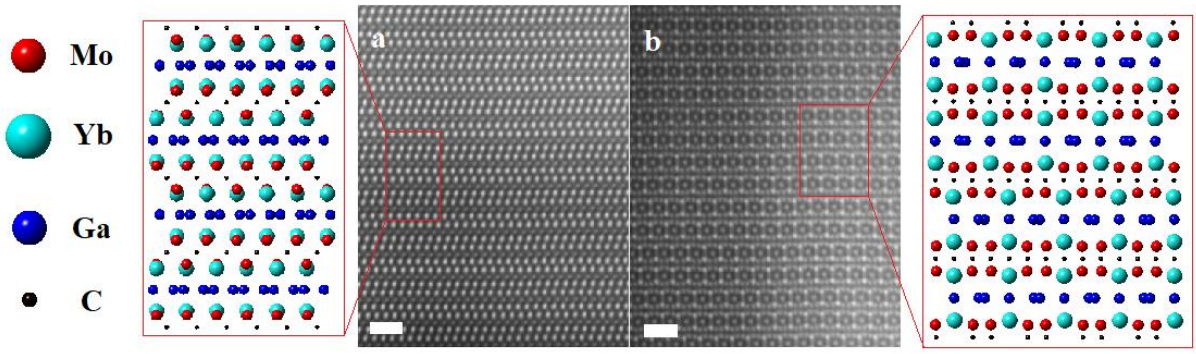

Figure 2. STEM micrographs of $(Mo_{2/3}Yb_{1/3})_2GaC$ sample along the a) [100], and in b) [110] zone axis, showing the monoclinic space group #15 structure (*C*2/*c*). Schematics next to each panel represent the corresponding atomic arrangements assuming a structure with monoclinic symmetry (*C*2/*c*). The scale bars in a) and b) are 1 nm.

Figure 3 shows the STEM micrographs of all synthesized $(Mo_{2/3}RE_{1/3})_2GaC$ *i*-MAX phases in the present study, with the chemical order of the *i*-MAX being evident when viewed along the [010] or [110] zone axis. Both (*C*2/*c*) and (*Cmcm*) symmetries are identified. Further STEM and SAED analysis is presented in Figure S3-S9. Furthermore, the relative composition of the phases, as obtained by SEM-EDX, can be found in table S2 in the supplemental information. Comparing the structures of all RE-based *i*-MAX phases identified to date, it can be noted

that a majority of those with A=Al are monoclinic, while those with A=Ga are primarily orthorhombic. The origin thereof is not clear, even though we find 3.5% higher values of *b* and *c* lattice parameters of the Al-based phases, compared to the Ga counterparts, while the *a* lattice parameters are larger for the Ga-based phases. The resulting difference in volume is about 1%, with larger values for the Al-based phases, consistent with the larger radius of Al compared to Ga.

It is also noted that there are no Ga-based *i*-MAX phases with light RE-elements, as opposed to the Al-based counterpart that can accommodate both light and heavy RE-elements. The reason for this observation can likely not be explained simply by elemental characteristics or preferred crystal structure, though it should be noted that the light RE elements of the Al phases crystallize in a monoclinic *C*2/*m* structure, whereas the heavier ones form the monoclinic *C*2/*c* structure. The former structure has not been identified for the here presented Ga-based phases.

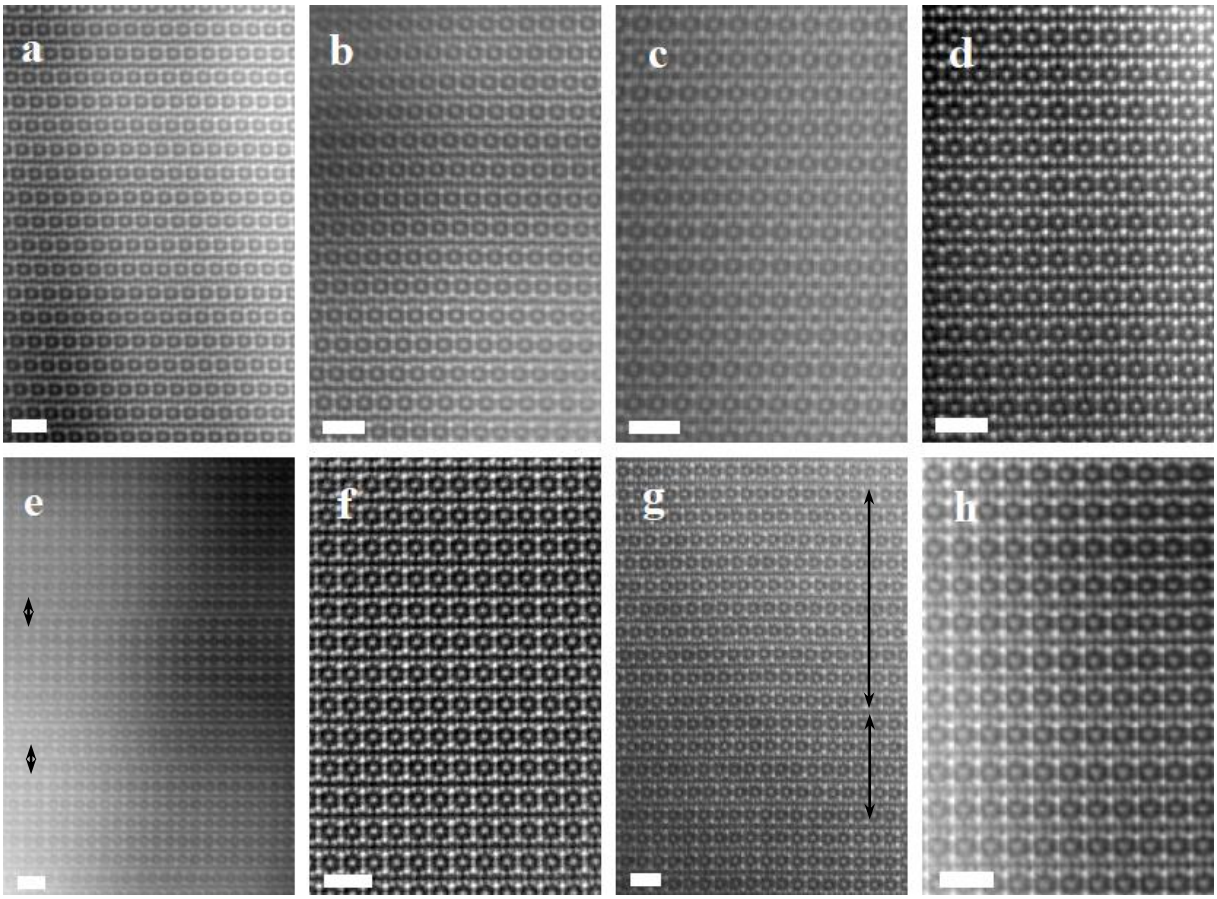

Figure 3. STEM micrographs of $(Mo_{2/3}RE_{1/3})_2GaC$ *i*-MAX phases showing the characteristic chemical order, as described primarily by a space group #63 (*Cmcm*) symmetry. The samples a) RE=Gd and b) RE=Tb are viewed along the [110] zone axis, showing a zig-zag-like pattern along with the chemical order. The samples c) RE=Dy, d) RE=Ho, f) RE=Tm and h) RE=Lu are viewed along the [010] zone axis. In e) and g), for the Er and Yb samples, respectively, both #63 (*Cmcm*) and #15 (*C*2/*c*) symmetries are present in a single grain (segments marked with arrows), thus this orientation corresponds to the [010] zone axis for (*Cmcm*) and the [110] zone axis for (*C*2/*c*). The scale bars in a)-h) are 1 nm.

Since the only difference between these eight new *i*-MAX phases is the change in RE element, our discovery allows systematic, fundamental studies of the effect of the RE element on the materials properties. Furthermore, the presence of RE elements with 4*f* electrons might

provide interesting magnetic properties, in line with the plethora of magnetic characteristics found in previous RE-containing *i*-MAX phases,[28] including magnetically frustrated systems due to inter- and intralayer interaction. Most of the RE-*i*-MAX phases reported herein, with A=Ga, have a counterpart in the previously reported corresponding compound $(Mo_{2/3}RE_{1/3})_2AlC$, with A=Al. Thus, the tuning potential of these materials is facilitated by both changes in the RE elements and the A layer. The latter is exemplified for MAX phases through previously observed altered magnetic transition temperature when going from $(Cr_{1-x}Mn_x)_2GaC$ [31] to $(Cr_{1-x}Mn_x)_2AlC$ [32]. Similar effects might be expected for the magnetic *i*-MAX phases. Furthermore, Ga is known to enhance the magnetostrictive properties of Fe [33], and also significant magnetostriction was found for the Mn_2GaC MAX phase [34]. Similar investigations of magnetic properties of the novel Ga-based materials of the present paper are therefore suggested.

Finally, Yb has previously been used in attempts to synthesize $(Mo_{2/3}Yb_{1/3})_2AlC$ [28], though not successful to date. The suggested explanation included the divalent nature of the Yb. Through the here presented synthesis of $(Mo_{2/3}Yb_{1/3})_2GaC$ *i*-MAX phase, Yb is a new M-element in the MAX phase family. The mechanism behind the formation of an Yb-based *i*-MAX phase for A=Ga, but not for A=Al, remains to be investigated, however, the interaction resulting from the divalent characteristics may be at least part of the explanation. This would suggest that also $(Mo_{2/3}Eu_{1/3})_2GaC$ exists, which was, however, not attempted in the present study.

Conclusions

Eight new *i*-MAX phases were realized based on RE as minority M element, of the formula

$(Mo_{2/3}RE_{1/3})_2GaC$ for RE = Gd, Tb, Dy, Ho, Er, Tm, Yb, and Lu. The compounds were found to crystallize in an orthorombic (*Cmcm*) structure, with the exception for RE=Ho and Yb, where also (*C*2/*c*) was found present in a small amount. The lattice parameters trendwise decrease by increasing atomic number going from Gd to Lu.

Acknowledgements

A.P. acknowledges Quanzheng Tao for provided help and support in Rietveld refinement. J.R. acknowledges support from the Swedish Foundation for Strategic Research (SSF) for Project Funding (EM16-0004), from the Knut and Alice Wallenberg (KAW) Foundation for a Fellowship Grant, Project funding (KAW 2015.0043), and for support to the Linköping Ultra Electron Microscopy Laboratory, and from the Swedish Government Strategic Research Area in Materials Science on Functional Materials at Linköping University (Faculty Grant SFO-Mat-LiU No 2009 00971). The Swedish Research council is also gratefully acknowledged through Project 642-2013-8020.

References

1. Nakatsuji S, Kiyohara N, Higo T. Large anomalous Hall effect in a non-collinear antiferromagnet at room temperature. Nature. 2015 10/28/online;527:212. doi: 10.1038/nature15723.
2. Essafi K, Benton O, Jaubert LDC. A kagome map of spin liquids from XXZ to Dzyaloshinskii–Moriya ferromagnet [Article]. Nat Commun. 2016 01/22/online;7:10297. doi: 10.1038/ncomms10297.
3. Riseborough PS. Heavy fermion semiconductors. Advances in Physics. 2000 2000/05/01;49(3):257-320. doi: 10.1080/000187300243345.
4. Dzero M, Xia J, Galitski V, et al. Topological Kondo Insulators. 2016;7(1):249-280. doi: 10.1146/annurev-conmatphys-031214-014749.
5. Xu Y, Yue C, Weng H, et al. Heavy Weyl Fermion State in $CeRu_4Sn_6$. Physical Review X. 2017 03/07/;7(1):011027. doi: 10.1103/PhysRevX.7.011027.
6. Flouquet J, Harima HJapa. Heavy fermion material: Ce versus Yb case. 2009.
7. Brando M, Belitz D, Grosche FM, et al. Metallic quantum ferromagnets. Reviews of Modern Physics. 2016 05/31/;88(2):025006. doi: 10.1103/RevModPhys.88.025006.

8. Wirth S, Steglich F. Exploring heavy fermions from macroscopic to microscopic length scales [Review Article]. Nature Reviews Materials. 2016 08/09/online;1:16051. doi: 10.1038/natrevmats.2016.51.
9. Ruderman MA, Kittel C. Indirect Exchange Coupling of Nuclear Magnetic Moments by Conduction Electrons. Phys Rev. 1954 10/01/;96(1):99-102. doi: 10.1103/PhysRev.96.99.
10. Kasuya T. A Theory of Metallic Ferro- and Antiferromagnetism on Zener's Model. Progress of Theoretical Physics. 1956;16(1):45-57. doi: 10.1143/PTP.16.45.
11. Yosida K. Magnetic Properties of Cu-Mn Alloys. Phys Rev. 1957 06/01/;106(5):893-898. doi: 10.1103/PhysRev.106.893.
12. Gertrud Z. Field-induced suppression of the heavy-fermion state in YbRh 2 Si 2. J Phys-Condens Mat. 2011;23(9):094215.
13. Tao Q, Dahlqvist M, Lu J, et al. Two-dimensional $Mo_{1.33}C$ MXene with divacancy ordering prepared from parent 3D laminate with in-plane chemical ordering [Article]. Nat Commun. 2017 Apr 25;8:14949. doi: 10.1038/ncomms14949. PubMed PMID: 28440271; PubMed Central PMCID: PMCPMC5413966.
14. Dahlqvist M, Lu J, Meshkian R, et al. Prediction and synthesis of a family of atomic laminate phases with Kagomé-like and in-plane chemical ordering. Sci Adv. 2017 Jul;3(7):e1700642. doi: 10.1126/sciadv.1700642. PubMed PMID: 28776034; PubMed Central PMCID: PMCPMC5517111.
15. Barsoum MW. MAX Phases: Properties of Machinable Ternary Carbides and Nitrides. 2013 September 2013.
16. Jeitschko W, Nowotny H, Benesovsky F. Kohlenstoffhaltige ternäre Verbindungen (V-Ge-C, Nb-Ga-C, Ta-Ga-C, Ta-Ge-C, Cr-Ga-C und Cr-Ge-C). Monatsh Chem. 1963;94(5):844-850. doi: 10.1007/bf00902358.
17. Barsoum MW. The $M_{N+1}AX_N$ phases: A new class of solids: Thermodynamically stable nanolaminates. Prog Solid State Chem. 2000;28(1–4):201-281. doi: http://dx.doi.org/10.1016/S0079-6786(00)00006-6.
18. Barsoum MW, El-Raghy T. The MAX Phases: Unique New Carbide and Nitride Materials: Ternary ceramics turn out to be surprisingly soft and machinable, yet also heat-tolerant, strong and lightweight. American Scientist. 2001;89(4):334-343.
19. Barsoum MW, Radovic M. Elastic and Mechanical Properties of the MAX Phases. Annu Rev Mater Sci. 2011;41(1):195-227. doi: doi:10.1146/annurev-matsci-062910-100448.
20. Hoffman EN, Vinson DW, Sindelar RL, et al. MAX phase carbides and nitrides: Properties for future nuclear power plant in-core applications and neutron transmutation analysis. Nucl Eng Des. 2012 2012/03/01/;244(Supplement C):17-24. doi: https://doi.org/10.1016/j.nucengdes.2011.12.009.
21. Fashandi H, Dahlqvist M, Lu J, et al. Synthesis of Ti_3AuC_2, $Ti_3Au_2C_2$ and Ti_3IrC_2 by noble metal substitution reaction in Ti_3SiC_2 for high-temperature-stable Ohmic contacts to SiC [Article]. Nature Materials. 2017 05/01/online;16:814. doi: 10.1038/nmat4896
https://www.nature.com/articles/nmat4896#supplementary-information.
22. Naguib M, Mashtalir O, Carle J, et al. Two-Dimensional Transition Metal Carbides. ACS Nano. 2012 2012/02/28;6(2):1322-1331. doi: 10.1021/nn204153h.
23. Anasori B, Lukatskaya MR, Gogotsi Y. 2D metal carbides and nitrides (MXenes) for energy storage [Review Article]. Nature Reviews Materials. 2017 01/17/online;2:16098. doi: 10.1038/natrevmats.2016.98
https://www.nature.com/articles/natrevmats201698#supplementary-information.
24. Dahlqvist M, Petruhins A, Lu J, et al. Origin of Chemically Ordered Atomic Laminates (*i*-MAX): Expanding the Elemental Space by a Theoretical/Experimental Approach. ACS Nano. 2018 Aug 28;12(8):7761-7770. doi: 10.1021/acsnano.8b01774. PubMed PMID: 30016074.
25. Meshkian R, Dahlqvist M, Lu J, et al. W-Based Atomic Laminates and Their 2D Derivative $W_{1.33}C$ MXene with Vacancy Ordering. 2018;30(21):1706409. doi: doi:10.1002/adma.201706409.
26. Lu J, Thore A, Meshkian R, et al. Theoretical and Experimental Exploration of a Novel In-Plane Chemically Ordered $(Cr_{2/3}M_{1/3})_2AlC$ *i*-MAX Phase with *M* = Sc and Y. Cryst Growth Des. 2017 2017/11/01;17(11):5704-5711. doi: 10.1021/acs.cgd.7b00642.

27. Persson I, el Ghazaly A, Tao Q, et al. Tailoring Structure, Composition, and Energy Storage Properties of MXenes from Selective Etching of In-Plane, Chemically Ordered MAX Phases. 2018;14(17):1703676. doi: doi:10.1002/smll.201703676.
28. Tao Q, Lu J, Dahlqvist M, et al. Atomically Layered and Ordered Rare-Earth i-MAX Phases: A New Class of Magnetic Quaternary Compounds. Chemistry of Materials. 2019 2019/04/09;31(7):2476-2485. doi: 10.1021/acs.chemmater.8b05298.
29. Rodríguez-Carvajal J. Recent advances in magnetic structure determination by neutron powder diffraction. Physica B: Condensed Matter. 1993 1993/10/01/;192(1):55-69. doi: https://doi.org/10.1016/0921-4526(93)90108-I.
30. Rodríguez-Carvajal J. Recent developments of the program FULLPROF. Commission on powder diffraction (IUCr) Newsletter. 2001;26:12-19.
31. Salikhov R, Semisalova AS, Petruhins A, et al. Magnetic Anisotropy in the $(Cr_{0.5}Mn_{0.5})_2GaC$ MAX Phase. Mater Res Lett. 2015 2015/07/03;3(3):156-160. doi: 10.1080/21663831.2015.1036324.
32. Mockute A, Persson POÅ, Magnus F, et al. Synthesis and characterization of arc deposited magnetic $(Cr,Mn)_2AlC$ MAX phase films. Phys Status Solidi RRL. 2014;8(5):420-423. doi: 10.1002/pssr.201409087.
33. Atulasimha J, Flatau AB. A review of magnetostrictive iron–gallium alloys. Smart Mater Struct. 2011 2011/03/08;20(4):043001. doi: 10.1088/0964-1726/20/4/043001.
34. Novoselova IP, Petruhins A, Wiedwald U, et al. Large uniaxial magnetostriction with sign inversion at the first order phase transition in the nanolaminated Mn_2GaC MAX phase. Sci Rep. 2018;8(1):2637.